

Lattice Boltzmann simulations of lamellar and droplet phases

G. Gonnella¹, E. Orlandini², and J.M. Yeomans³

¹*Dipartimento di Fisica dell'Universita' di Bari and Istituto Nazionale di Fisica Nucleare,
Sezione di Bari, via Amendola 173, 70126 Bari, Italy.*

²*Service de Physique Theorique, Centre d'etudes de Saclay, F-91191 Gif-sur-Yvette, France.*

³*Theoretical Physics, Oxford University, 1 Keble Rd., Oxford OX1 3NP, UK.*

(March 21, 2018)

Abstract

Lattice Boltzmann simulations are used to investigate spinodal decomposition in a two-dimensional binary fluid with equilibrium lamellar and droplet phases. We emphasise the importance of hydrodynamic flow to the phase separation kinetics. For mixtures slightly asymmetric in composition the fluid phase separates into bulk and lamellar phases with the lamellae forming distinctive spiral structures to minimise their elastic energy.

PACS numbers: 47.11.+j; 64.75.+g

I. INTRODUCTION

Complex fluids such as microemulsions, foams, and colloidal suspensions provide a wealth of interesting physical phenomena. Their use is ubiquitous in the processing, energy and chemical industries. Therefore it is important to explore ways in which their properties can be modelled numerically to test physical theories, predict behaviour and provide feedback to industrial planning.

The modelling of complex fluids is not an easy task as both the rheology and the complicated phase behaviour of the fluid must be incorporated. Molecular dynamics simulations, whilst providing an accurate picture of the microscopic physics, are usually too computer-intensive to address hydrodynamic time scales. In computational fluid dynamic solutions of the Navier-Stokes equations the specific behaviour of a given fluid can only be input via ad hoc constitutive relations.

Recently new methods of simulating fluid flow have become available. These include lattice-gas cellular automata¹, dissipative particle dynamics², and lattice Boltzmann simulations³. The aim is to reproduce the physics of fluid flow, primarily mass and momentum conservation, while including the important features of the underlying microscopic physics. These approaches have been successfully applied to several complex fluids including polymer solutions⁴, particulate suspensions⁵ and microemulsions¹. However application of the techniques to model complex fluids is still in its infancy and validation of, and comparison between, the different methods is still needed.

In this paper we concentrate on lattice Boltzmann simulations. A fluid is modelled on a mesoscopic length scale by means of distribution functions which evolve according to a discretised version of a simplified Boltzmann equation. The correct equilibrium behaviour is imposed by inputting the correct thermodynamics such that the system evolves to the minimum of a chosen input free energy^{6,7}.

We use the lattice Boltzmann approach to explore the kinetics of phase separation of a model, two-dimensional, fluid with lamellar and droplet equilibrium phases. Our main

conclusions are:

1. When the system is quenched to the lamellar phase a glassy metastable state of tangled lamellae forms. However, hydrodynamic flow alleviates the frustration and allows the system to attain the striped ground state.
2. As the concentration of the minority phase is increased the system prefers to phase separate into a lamellar and a one-component phase. The lamellae minimise their free energy by forming a spiral pattern around the one-component hole. Again this state can only be reached by the fluid if hydrodynamic flow is allowed in the system.
3. When one component of the binary fluid predominates droplets of the minority fluid form. Their size is determined by the balance of the surface tension terms in the free energy. Phase separation in this system is unaffected by hydrodynamics.

Sections 2 and 3 of the paper are devoted to a description of the model and the relevant thermodynamics and to a summary of the numerical approach respectively. Section 4 summarises phase separation in a 50:50 fluid mixture emphasising the rôle of hydrodynamics. The 60:40 mixture which phase separates into a lamellar and one-component state is considered in Section 5. Section 6 treats the 90:10 composition ratio where droplets of the minority phase are stable. Section 7 summarises the results, putting them in the context of previous work, and suggests directions for future research.

II. MODEL

We consider a two-dimensional binary fluid with components A , B of number density n_A , n_B respectively. This can be modelled by the Landau free energy⁸

$$\Psi = \int d\vec{r} \left\{ \frac{a}{2}(\varphi)^2 + \frac{b}{4}(\varphi)^4 + \frac{\kappa}{2}(\nabla\varphi)^2 + \frac{\zeta}{2}(\nabla^2\varphi)^2 \right\} \quad (1)$$

where $\varphi = n_A - n_B$ is the order parameter of the system and we assume that the total density $n = n_A + n_B$ is constant. The free energy (1) corresponds to a disordered state at high temperatures ($a > 0$) and an ordered state at low temperatures ($a < 0$).

κ is related to the surface tension. For κ sufficiently large the ordered phase consists of two coexisting bulk phases with $n_A - n_B = \pm\varphi_0$, the volume of each determined by the initial ratio of n_A and n_B . As κ is decreased the formation of interfaces becomes favourable but the fluid remains stable because of the positive curvature energy related to ζ in (1). For $n_A \sim n_B$ the ordered state is then a striped or lamellar phase with the width of the lamellae being determined by the interface–interface interaction. For $n_A \ll n_B$ this is replaced by a phase of circular droplets of A in B with radius determined by the balance between the negative surface tension and the positive curvature free energies of the interfaces.

Thermodynamic properties of the binary fluid follow directly from the free energy (1). In particular we shall need the chemical potential $\Delta\mu$ which couples to the density difference φ

$$\Delta\mu = \frac{\delta\psi}{\delta\varphi} = a\varphi + b\varphi^3 - \kappa\nabla^2\varphi + \zeta(\nabla^2)^2\varphi. \quad (2)$$

Obtaining the pressure tensor is slightly more complicated⁹. The pressure parallel to the interface follows from (1)

$$p_L = \frac{a}{2}\varphi^2 + \frac{3b}{4}\varphi^4 - \kappa\varphi(\nabla^2\varphi) - \frac{\kappa}{2}(\nabla\varphi)^2 + \zeta\varphi(\nabla^2)^2\varphi - \frac{\zeta}{2}(\nabla^2\varphi)^2. \quad (3)$$

However off-diagonal terms must be added to ensure that the pressure tensor obeys the equilibrium condition

$$\partial_\alpha P_{\alpha\beta} = 0. \quad (4)$$

Considering a linear combination of all symmetric tensors having two or four gradient operators shows that a suitable choice is

$$\begin{aligned} P_{\alpha\beta} = & \{p_L + \zeta(\nabla^2\varphi)^2 + \zeta\partial_\gamma\varphi\partial_\gamma(\nabla^2\varphi)\}\delta_{\alpha\beta} \\ & + \kappa\partial_\alpha\varphi\partial_\beta\varphi - \zeta\left\{\partial_\alpha\varphi\partial_\beta(\nabla^2\varphi) + \partial_\beta\varphi\partial_\alpha(\nabla^2\varphi)\right\}. \end{aligned} \quad (5)$$

III. LATTICE BOLTZMANN SIMULATIONS

The aim is to simulate a fluid with equilibrium properties described by the free energy (1) which obeys the Navier-Stokes and convection-diffusion equations. To this end we use a lattice Boltzmann technique⁷.

We consider a square lattice and define two sets of distribution functions $\{f_i\}$ and $\{g_i\}$ on each lattice site \vec{x} . Each f_i, g_i is associated with a lattice vector \vec{e}_i . The results presented in this paper are for a 9-velocity model on a square lattice with $e_i/c = (\pm 1, 0), (0, \pm 1), (\pm 1/\sqrt{2}, \pm 1/\sqrt{2}), (0, 0)$.

Physical variables are related to the distribution functions through

$$n = \sum_i f_i, \quad nu_\alpha = \sum_i f_i e_{i\alpha}, \quad (6)$$

$$\varphi = \sum_i g_i \quad (7)$$

where \vec{u} is the mean fluid velocity.

The distribution functions undergo a collision step followed by a streaming step according to the evolution equations

$$f_i(\vec{x} + \vec{e}_i \Delta t, t + \Delta t) - f_i(\vec{x}, t) = -\frac{1}{\tau_1} (f_i - f_i^0), \quad (8)$$

$$g_i(\vec{x} + \vec{e}_i \Delta t, t + \Delta t) - g_i(\vec{x}, t) = -\frac{1}{\tau_2} (g_i - g_i^0) \quad (9)$$

where Δt is the time step, τ_1 and τ_2 are relaxation parameters, and f_i^0 and g_i^0 are equilibrium distribution functions the choice of which determines the physics inherent in the simulation. Equations (8) and (9) are discrete Boltzmann equations with a BGK collision term¹⁰.

Following the standard lattice Boltzmann prescription we assume that f_i^0 and g_i^0 can be expanded as power series in the bulk velocity

$$f_i^0 = A + B u_\alpha e_{i\alpha} + C u^2 + D u_\alpha u_\beta e_{i\alpha} e_{i\beta} + G_{\alpha\beta} e_{i\alpha} e_{i\beta}, \quad (10)$$

$$f_0^0 = A_0 + C_0 u^2, \quad (11)$$

$$g_i^0 = H + Ku_\alpha e_{i\alpha} + Ju^2 + Qu_\alpha u_\beta e_{i\alpha} e_{i\beta}, \quad (12)$$

$$g_0^0 = H_0 + J_0 u^2. \quad (13)$$

The expansion coefficients $A, B \dots$ are determined by

$$\sum_i f_i^0 = n \quad (14)$$

$$\sum_i f_i^0 e_{i\alpha} = nu_\alpha, \quad (15)$$

$$\sum_i f_i^0 e_{i\alpha} e_{i\beta} = P_{\alpha\beta} + nu_\alpha u_\beta, \quad (16)$$

$$\sum_i g_i^0 = \varphi, \quad (17)$$

$$\sum_i g_i^0 e_{i\alpha} = \varphi u_\alpha, \quad (18)$$

$$\sum_i g_i^0 e_{i\alpha} e_{i\beta} = \Gamma \Delta\mu \delta_{\alpha\beta} + \varphi u_\alpha u_\beta. \quad (19)$$

where $P_{\alpha\beta}$ and $\Delta\mu$ are given by (5) and (2) respectively and Γ is a mobility. Note that the conditions (14), (15), and (17) correspond to local conservation of density, momentum and density difference respectively. Explicit expressions for the expansion coefficients are given in Appendix A.

Expanding (8) and (9) to order $(\Delta t)^2$ and using (14)–(19) leads to the macroscopic equations

$$\partial_t n + \partial_\alpha (nu_\alpha) = 0, \quad (20)$$

$$\partial_t (nu_\beta) + \partial_\alpha (nu_\alpha u_\beta) = -\partial_\alpha P_{\alpha\beta} + \nu \nabla^2 (nu_\beta) + \partial_\beta \{ \lambda(n) \partial_\alpha (nu_\alpha) \}, \quad (21)$$

$$\partial_t \varphi + \partial_\alpha (\varphi u_\alpha) = \Gamma \theta \nabla^2 \Delta\mu - \theta \partial_\alpha \left(\frac{\varphi}{n} \partial_\beta P_{\alpha\beta} \right), \quad (22)$$

where

$$\theta = (\Delta t)c^2 (\tau_2 - 1/2), \nu = \frac{(2\tau_1 - 1)}{6}(\Delta t)c^2, \lambda(n) = (\tau_1 - \frac{1}{2})\Delta t(\frac{c^2}{2} - \frac{dp_0}{dn}). \quad (23)$$

It is apparent from these equations of motion that the fluid will evolve through two competing growth mechanisms. The first of these is diffusion, described by eqn. (22) with $\vec{u} = 0$. The second is bulk momentum transfer or hydrodynamic flow described by the Navier-Stokes equation (21). The relative importance of diffusive and hydrodynamic flow can be altered by varying the viscosity ν through changes in τ_1 (see equation (23)). For high viscosities the velocities remain sufficiently small that hydrodynamic flow is irrelevant and the evolution of the microstructure is diffusive. For low viscosities, however, the Reynolds number becomes larger and hydrodynamic effects can dominate in changing the domain morphology. Simulations run from the same initial conditions but with high or low viscosities enable us to build up a very clear picture of the effects of hydrodynamics on the domain growth.

IV. 50:50 COMPOSITION: METASTABILITY AND THE EFFECT OF HYDRODYNAMICS

We first describe the behaviour of a symmetric binary fluid with a ratio of number densities $n_A : n_B$ of 50 : 50 when it is quenched from a disordered state into the ordered region. Our aim is to compare the path of the spinodal decomposition for different values of the surface tension and of the viscosity. Initial results for this concentration have appeared elsewhere¹¹.

For all runs the system was initialised with $n = 1.0$ and φ chosen randomly between -0.5 and 0.5 . It was then quenched to a final state defined by parameters $a = -1, b = \zeta = 1$. The simulations were run with $\Delta t = 0.004, c = 1, \tau_2 = 0.7786751$ and $\Gamma = 1$. The system size was 128×128 and simulations were typically run for 10^5 time steps. This took approximately 10 days on a DEC Alpha Workstation. Smaller lattice sizes gave similar results.

For κ sufficiently negative the equilibrium state is a lamellar phase. After a quench at high viscosity the fluid gets stuck in a metastable state of lamellae which have approximately the correct width, but which are tangled. For low viscosity, however, hydrodynamic flow builds up and can remove topological defects from the system and allow the fluid to reach equilibrium.

Evidence for these conclusions is shown in Figure 1 where snapshots of the domain growth are compared for three different sets of parameters:

- (a) high viscosity, two-phase coexistence ($\tau_1 = 50$, $\kappa = 0.1$),
- (b) high viscosity, lamellar equilibrium ($\tau_1 = 50$, $\kappa = -0.85$),
- (c) low viscosity, lamellar equilibrium ($\tau_1 = 0.585$, $\kappa = -0.85$).

Consider first (a) which is at a value of κ that corresponds to bulk phase separation and a value of τ_1 that suppresses hydrodynamic flow. After initial transients sharp domains form. These are more elongated than for a system with $\zeta = 0$ but they grow continuously and become more isotropic. An exponent α characterising the growth is commonly defined by

$$R(t) \sim t^\alpha \tag{24}$$

where $R(t)$ is a length scale, which we take as the inverse of the first moment of the circularly averaged structure factor, and t is the time¹². At late times α converges to $1/3$ as expected for Lifshitz-Slyozov diffusive growth in a binary system. Runs at different values of κ indicate that as κ is decreased an increasingly long time is taken to reach the $1/3$ regime¹¹.

For $\kappa < \kappa_c \sim -0.8$ there is a qualitative change in the behaviour of the system as shown in Figure 1b. These results were obtained for the same value of τ_1 but with $\kappa = -0.85$ where the equilibrium is the lamellar state. Now the system forms portions of lamellae of width approximately equal to the equilibrium value. These lamellae are tangled in a way that depends on the initial conditions. The diffusive growth to the tangled phase is

slow, possibly logarithmic, and once the glassy phase has been reached there is no further discernable movement on the time-scale of the simulation. For smaller κ the lamellae are thinner and the system freezes sooner.

Remaining with the value $\kappa = -0.85$ we then ran the same simulation (starting from the same initial conditions) for $\tau_1 = 0.585$. The lower value of τ implies a lower viscosity and the possibility of hydrodynamic flow at earlier times. The initial behaviour was the same as for case (b) with a glassy lamellar phase being formed. However at a later time t there was a significant change in the domain pattern. This is most easily seen from the snapshots in Figure 1c where it is apparent that the topological frustration of the glassy phase is being removed and the lamellae are lining up in the global equilibrium state.

An example of the effect of hydrodynamic flow on the defects is shown in Figure 2. The lamellae are initially too wide. Hydrodynamic forces tend to lengthen them causing the broken lamellar to join and the stripes to buckle. At high viscosities the defect does not disappear.

V. 60:40 COMPOSITION: SEPARATION TO COEXISTING LAMELLAR AND BULK PHASES

We next consider a concentration ratio $n_A : n_B = 60 : 40$. Now there is too little of the B -phase to form lamellae of the correct width throughout the system. We shall show that the equilibrium state corresponds to phase separation into a lamellar region coexisting with a bulk A -phase. As before equilibrium can only be reached with the help of hydrodynamic flow.

Simulations were again run at different values of τ_1 and κ to provide a comparison. Snapshots of the time evolution are shown in Figure 3 for the same parameters as those used for the symmetric mixture considered in Section IV. Figure 4 is a double logarithmic plot of the variation of the domain size with time comparing the growth in the three different cases.

Column (a) of Figure 3 shows the path to bulk phase separation for $\kappa = 0.1$. Droplets form by spinodal decomposition and then grow by Lifshitz-Slyozov diffusion. The curvature term in the free energy becomes less important for larger droplets and they become more circular. The data in Figure 4 is consistent with the expected growth exponent $\alpha = 1/3$ at late times.

Figure 3b compares a simulation for $\kappa = -0.85$, a value for which the lamellar phase is stable in the symmetric mixture. The value of τ_1 is chosen so that only diffusive growth is possible. It is apparent from Figure 3b that the final state is a mixture of droplets and short lamellae. There are no further discernable changes in morphology on the time scale of the simulation as confirmed in Figure 4.

Evidence that this droplet state is metastable is provided when the same simulation is run with a low viscosity. Bulk fluid flow now allows the droplets to join to form lamellae and align. A surprising amount of movement is seen leading to the growth process shown in Figure 3c. In Figure 4 the onset of hydrodynamic flow in this system is marked by a rather sharp increase in the measured length scale.

The final state is coexistence between a lamellar and a bulk A-phase. The lamellae order in a distinctive spiral around the hole of A-phase, to minimise the elastic free energy which would be generated by incorrect lamellar spacings.

Finally we remark that very similar results were obtained for a concentration ratio of $n_A : n_B = 70 : 30$.

VI. 90:10 COMPOSITION: THE DROPLET PHASE

Finally we describe phase separation in a highly asymmetric binary fluid with $n_A : n_B = 90 : 10$. Now the equilibrium for κ sufficiently negative comprises droplets of B in A . Figure 5 compares results for two different values of κ :

- (a) high viscosity, two-phase coexistence ($\tau_1 = 50$, $\kappa = 0.1$)
- (b) high viscosity, lamellar equilibrium ($\tau_1 = 50$, $\kappa = -0.85$)

The main difference between the growth processes in Figures 5a and 5b is a direct consequence of the final equilibrium state. For $\kappa = 0.1$, once the domains have formed they continue to grow slowly by the diffusion of material between them. This is the Lifshitz-Slyozov growth process, driven by the difference in chemical potential between droplets of different size. For $\kappa = -0.85$ however there is a preferred size for droplets, set by the competition between the surface tension and the curvature energy, and growth stops once the droplets have reached this size. A second difference is that for the negative value of κ droplets form much more quickly in the early stages of growth. This is a consequence of the reduced surface tension.

Runs for a low viscosity and negative κ showed a negligible influence of hydrodynamics on growth for this concentration. This is as expected. Hydrodynamic flow can act to make a droplet circular because of the pressure difference between points of different curvature. However once the drops are circular hydrodynamic flow cannot directly lead to droplet coalescence although it may speed up the diffusive growth¹³.

VII. CONCLUSIONS

We have shown that there is a wealth of interesting behaviour as even rather simple structured fluids attain equilibrium. Competition between diffusive and hydrodynamic modes lead to final states dependent on the dynamic parameters of the system. In particular we have emphasised that hydrodynamic flow is often important in allowing a system to reach its equilibrium state.

The results were obtained using lattice Boltzmann simulations. The approach has two particular advantages in this context. Firstly equilibrium is determined by a free energy which is an intrinsic part of the simulation so the structure of the equilibrium state can be chosen rather naturally. Secondly the viscosity of the fluid can be tuned over a wide range. We caution however that the lattice Boltzmann evolution is not described by an H-theorem and thus no proof exists that the path to equilibrium is a physical one.

Lattice Boltzmann simulations do not intrinsically include noise although this can be added in an ad hoc way. An important question is whether such fluctuations can relax the disordered lamellar states. We ran simulations aimed at investigating this but found no effect of noise on the glassy structure. In real two-dimensional smectics fluctuations destroy the lamellar order. However, for this model we expect a stable lamellar phase, both because of the lack of fluctuations and because we impose a mean-field free energy.

Our conclusions are in broad agreement with those of Bahiana and Oono¹⁴ who considered the spinodal decomposition of a model of block copolymers designed to give a lamellar equilibrium. Despite the long-range interactions in the model a tangled lamellar phase was formed after a quench. This could be ordered by including terms approximating hydrodynamic flow in the simulation. Other related work¹⁵ uses a Langevin approach which includes hydrodynamics to model phase separation in microemulsions. The domain growth slows as the surfactant density is increased. This method provides an alternative numerical way to study complex fluids and it would be interesting to gain a fuller understanding of the applicabilities of the different approaches.

There are many questions that remain to be considered. These include the effect of confinement or shear on the phase separation, dynamical asymmetry in the viscosities of the two fluid components, and the rôle of a very low diffusivity, which has been shown to alter the path to bulk phase separation in binary fluids¹⁶. Work is in progress to include a surfactant as a third phase rather than modelling its effect by changing the surface tension. Extensions to three dimensions are highly desirable. These are feasible but at the limit of current numerical resources.

Acknowledgements

We should like to thank P.V. Coveney and A. Wagner for helpful comments. JY acknowledges support from the EPSRC (grant no. GR/K97783) and NATO (grant no. CRG950356).

APPENDIX A

A suitable choice of the coefficients in the expansions of the lattice Boltzmann equilibrium distributions (10)–(13) consistent with the conditions (14)–(19) is

$$\begin{aligned}
 A &= \frac{5}{4} \left(\frac{a}{2} \varphi^2 + \frac{3b}{4} \varphi^4 - \kappa \varphi (\nabla^2 \varphi) + \xi \varphi (\nabla^2)^2 \varphi + \frac{\zeta}{2} (\nabla^2 \varphi)^2 \right) / (12c^2), \\
 A_0 &= n - 16A, \quad B = 5n / (12c^2), \\
 C_0 &= -2n / (3c^2), \quad C = -5n / (24c^2), \quad D = 5n / (8c^4), \\
 G_{xx} = -G_{yy} &= \frac{5\kappa}{2} \left((\partial_x \varphi)^2 - (\partial_y \varphi)^2 \right) / 8c^4 + 5\zeta (\partial_y \varphi \partial_y (\nabla^2 \varphi) - \partial_x \varphi \partial_x (\nabla^2 \varphi)) / 8c^4, \\
 G_{xy} &= 5\kappa \partial_x \varphi \partial_y \varphi - 5\zeta \{ \partial_x \varphi \partial_y (\nabla^2 \varphi) + \partial_y \varphi \partial_x (\nabla^2 \varphi) \}, \\
 H_0 &= \varphi - 4H, \quad H = 5\Gamma \Delta \mu / (12c^2), \quad K = 5\varphi / (12c^2), \\
 J_0 &= -2\varphi / (3c^2), \quad J = -5\varphi / (24c^2), \quad Q = 5\varphi / (8c^2). \tag{25}
 \end{aligned}$$

REFERENCES

- ¹ A.N. Emerton, P.V. Coveney and B.M. Boghosian, Phys. Rev. E. **56** 1286 (1997).
- ² P.J. Hoogerbrugge and J.M.V.A. Koelman, Europhys. Lett. **19** 155 (1992).
- ³ R. Benzi, S. Succi and M. Vergassola, Phys. Rep. **222** 145 (1992). D.H. Rothman and S. Zaleski, Rev. Mod. Phys. **66** 1417 (1994).
- ⁴ A.G. Schlijper, P.J. Hoogerbrugge and C.W. Manke, J. Rheol. **39** 567 (1995).
- ⁵ E.S. Boek, P.V. Coveney and H.N.W. Lekkerkerker, J. Phys. Condens. Matter, **8** 9509 (1996).
- ⁶ M.R. Swift, W.R. Osborn and J.M. Yeomans, Phys. Rev. Lett. **75** 830 (1995).
- ⁷ E. Orlandini, M.R. Swift and J.M. Yeomans, Europhys. Lett. **32** 463 (1995). M.R. Swift, E. Orlandini, W.R. Osborn, and J.M. Yeomans, Phys. Rev. E. **54** 5041 (1996).
- ⁸ S.A. Brazovskii, Sov. Phys. JETP **41** 85 (1975).
- ⁹ A.J.M. Yang, P.D. Fleming and J.H. Gibbs, J. Chem. Phys. **64** 3732 (1976).
- ¹⁰ P.L. Bhatnager, E.P. Gross and M. Krook, Phys. Rev. **94** 511 (1954).
- ¹¹ E. Orlandini, G. Gonnella and J.M. Yeomans, Phys. Rev. Lett. **78** 1695 (1997).
- ¹² A.J. Bray, Adv. in Phys. **43** 357 (1994).
- ¹³ H. Tanaka, Phys. Rev. Lett. **72** 3690 (1994).
- ¹⁴ M. Bahiana and Y. Oona, Phys. Rev. A. **41** 6763 (1990).
- ¹⁵ G. Patzold and K. Dawson Phys. Rev. E. **52** 6908 (1995).
- ¹⁶ H. Tanaka, J. Chem. Phys. **103** 2361 (1995).

FIGURES

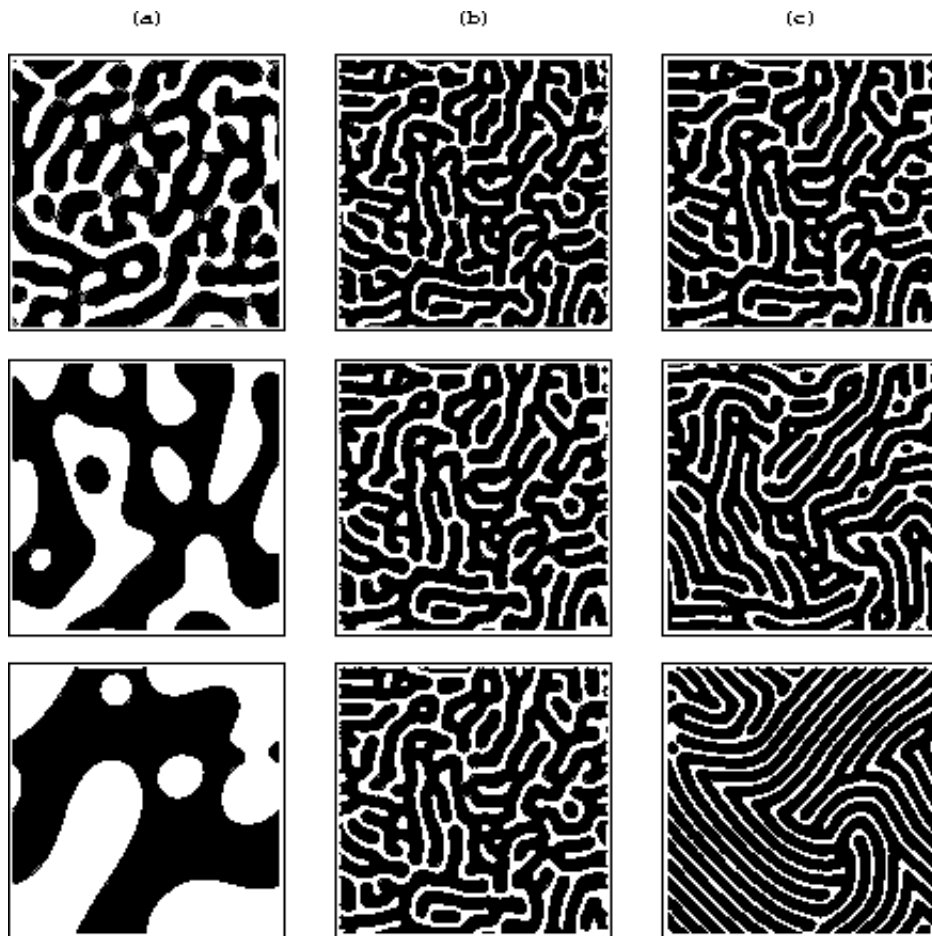


FIG. 1. Snapshots of the growth of domains with time for a binary mixture symmetric in composition. Grey-scaling from black \Rightarrow white corresponds to $\varphi = -1 \Rightarrow \varphi = 1$. Each column represents a different physical situation: (a) a quench to the homogeneous two-phase region $\kappa > \kappa_c$; (b) a quench to the lamellar phase $\kappa < \kappa_c$ in a high viscosity fluid. The lamellae form in a tangled pattern which becomes frozen in time; (c) a quench to the same value of κ as (b) but for a low viscosity fluid. Hydrodynamic modes allow the lamellae to reorder giving, locally, well-defined striped regions.

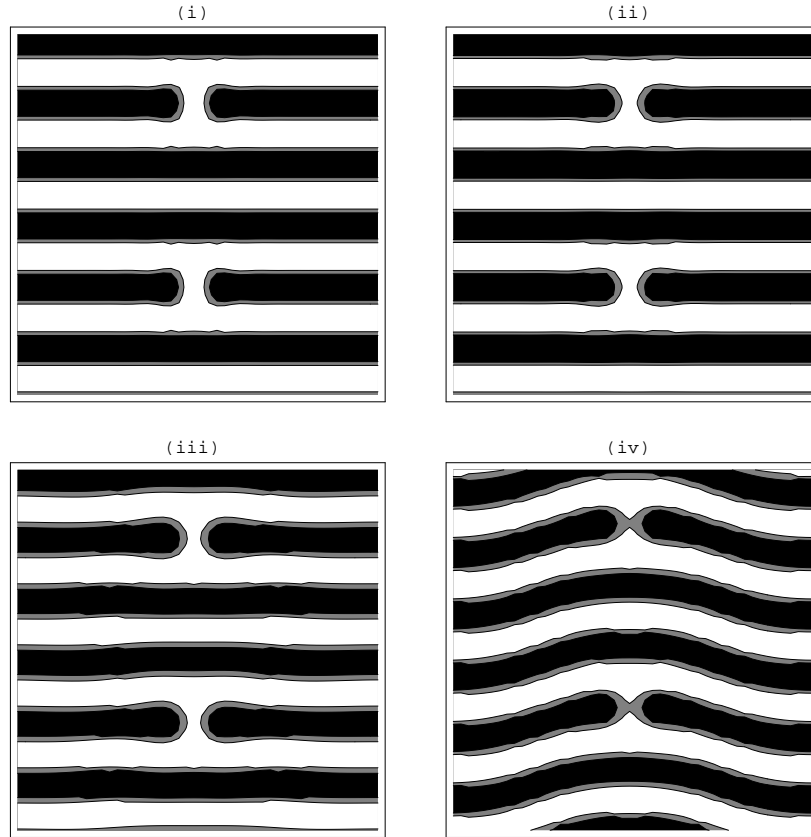


FIG. 2. Defect being removed by flow. The lamellae are initially too wide. Hydrodynamic forces tend to lengthen them causing the broken lamellar to join and the stripes to buckle. Grey-scaling from black \Rightarrow white corresponds to $\varphi = -1 \Rightarrow \varphi = 1$.

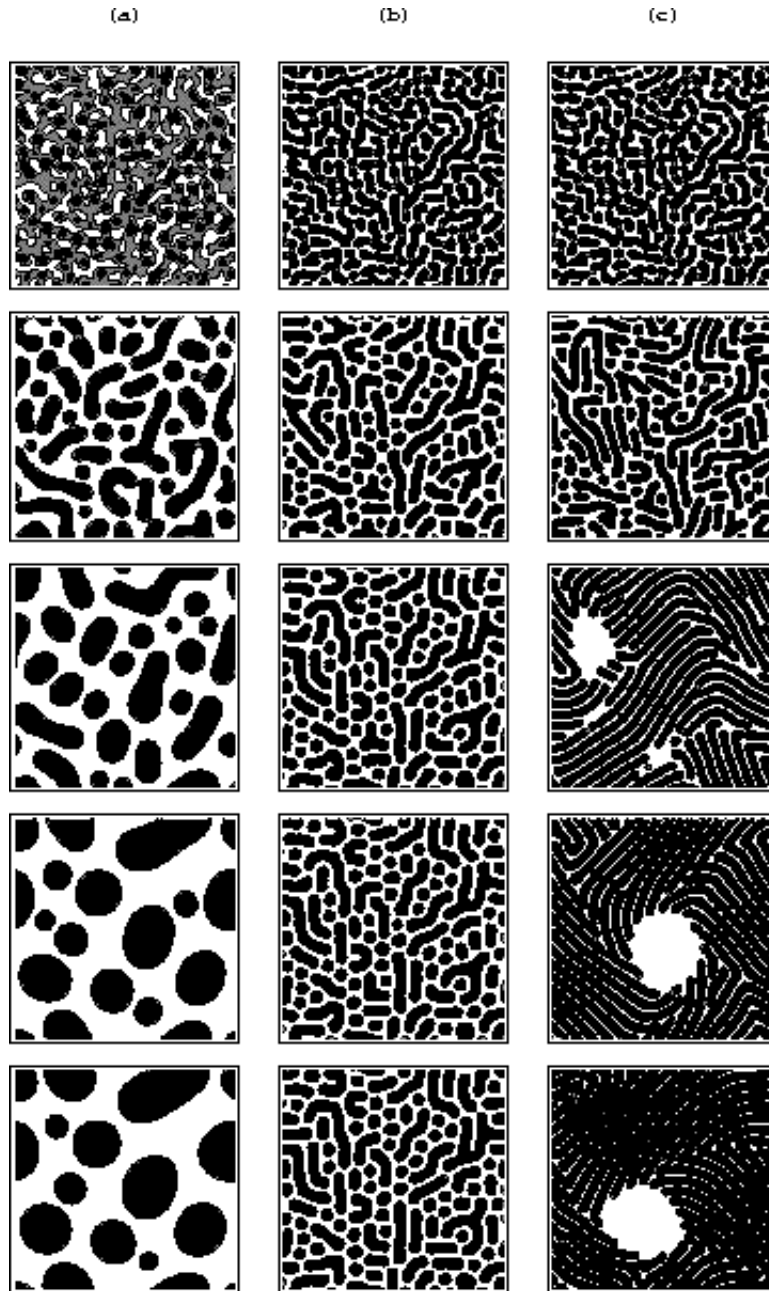


FIG. 3. Snapshots of the growth of domains with time for a binary mixture slightly asymmetric in composition. Grey-scaling from black \Rightarrow white corresponds to $\varphi = -1 \Rightarrow \varphi = 1$. (a) A quench to the homogeneous two-phase region $\kappa > \kappa_c$; (b) a quench to the lamellar phase $\kappa < \kappa_c$ in a high viscosity fluid. Short lamellae form in a pattern which becomes frozen on the time scale of the simulation; (c) a quench to the same value of κ as (b) but for a low viscosity fluid. Hydrodynamic flow allows the system to attain its equilibrium of coexisting lamellar and bulk- A phases.

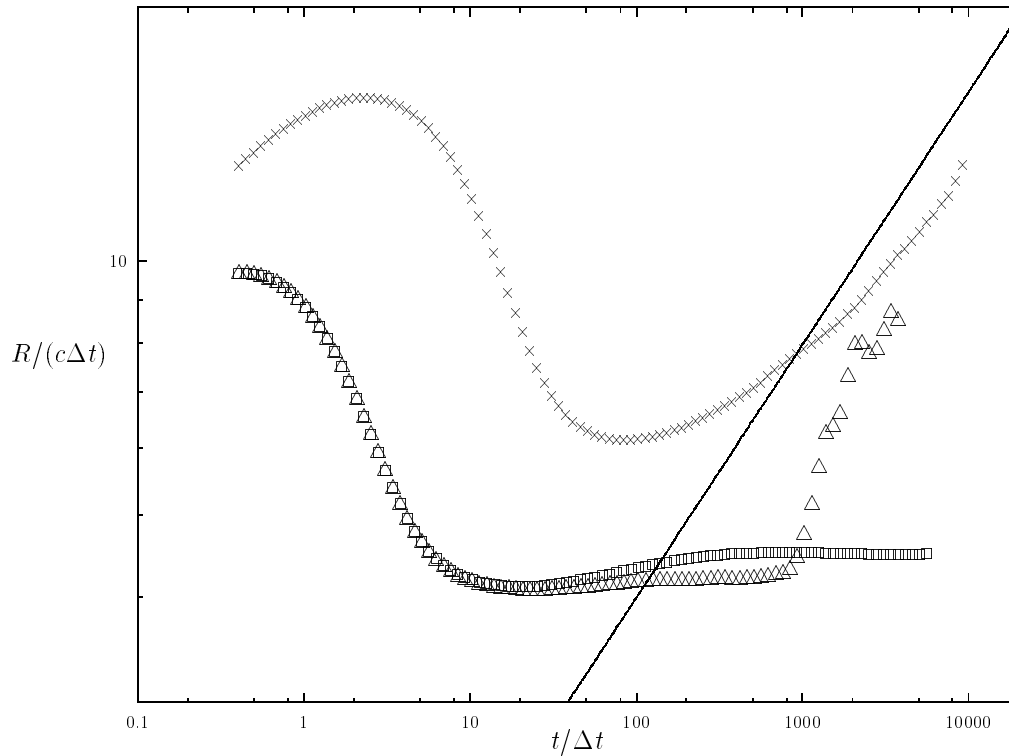


FIG. 4. Double logarithmic plot of the evolution of the inverse first moment of the structure factor as a function of time for each of the simulations shown in Figure 3: (\times) bulk phase separation, (\square) a quench to the lamellar phase with high viscosity, (\triangle) a quench to the lamellar phase with low viscosity. The straight line has slope 1/3. ¹

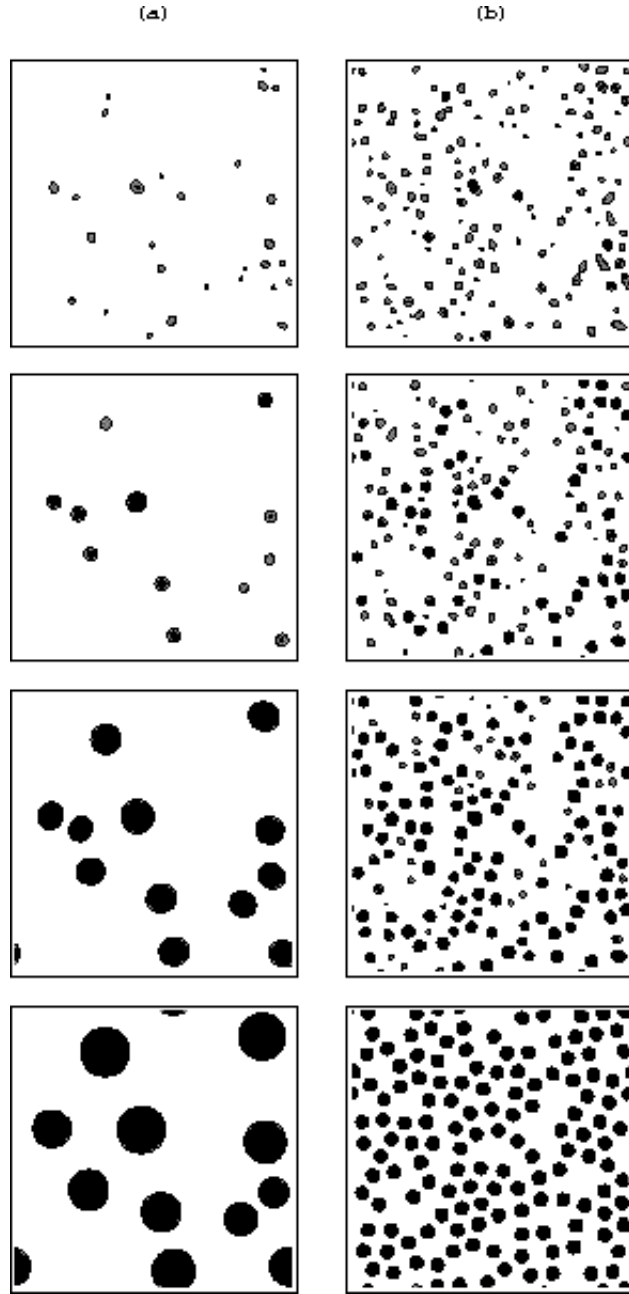


FIG. 5. Snapshots of the growth of domains with time for a binary mixture highly asymmetric in composition. Grey-scaling from black \Rightarrow white corresponds to $\varphi = -1 \Rightarrow \varphi = 1$. (a) A quench to the homogeneous two-phase region $\kappa > \kappa_c$; (b) a quench to the droplet phase $\kappa < \kappa_c$ where the final length scale is set by the competition between the surface tension and the curvature energy.